ANALYSIS OF PHASE ANGLE PROPERTIES AND SIMULATION OF EARTHQUAKE STRONG MOTIONS

by

Tetsuo Kubo (I)

SUMMARY

When analyzing earthquake strong motion records through the Fourier transformation, the signals involving significant properties of the waveform are divided into two halves. One is expressed in terms of the Fourier amplitudes, and the other in terms of the Fourier phase angles. Research works so far conducted extensively have focussed their interest primarily upon amplitude properties. In this paper, paying attention to phase angle properties, synthetic earthquake strong motions are generated. The cumulative energy quantities and elastic responses are evaluated for these motions, and the significance of phase angle properties is discussed.

INTRODUCTION

A strong motion record obtained during an earthquake shaking is a time function representing acceleration of motion at every moment. A time function representing physical phenomena will generally be integrable. It leads to the evidence that an earthquake record and its corresponding Fourier transform will uniquely be related with each other through the Fourier pair;

$$f(t) \leftrightarrow F(\omega) \qquad (1)$$

where $f(t)$ and $F(\omega)$ denote a time function of strong motion record and its Fourier transform, respectively. Equation (1) can be expressed by a pair of Fourier amplitude function $A(\omega)$ and Fourier phase angle function $\Phi(\omega)$ through

$$F(\omega) = A(\omega) \exp[-j\Phi(\omega)] \qquad (2)$$

Equations (1) and (2) signify that a pair of Fourier functions $A(\omega)$ and $\Phi(\omega)$ will uniquely be determined by time function $f(t)$, and vice versa.

Signals of a time function of earthquake strong motion record are divided equally into two halves. One of halves is given for Fourier amplitude properties $A(\omega)$, and the other for Fourier phase angle properties $\Phi(\omega)$.

Studies upon earthquake strong motion records so far carried out extensively, however, have focussed their interest upon relation between characteristics of earthquake motion records and those of their Fourier amplitude quantities. A few [1,2,3] have placed their emphasis upon the Fourier phase angles. It is the purpose of this study presented herein to reveal the significance of Fourier phase angle properties upon an earthquake strong motion, and apply phase angle properties obtained from analysis upon real earthquake strong motion records in simulation of realistic earthquake motions in an attempt to make application of synthetic motions in an engineering practice.

(I) Associate Professor, Department of Architecture, Faculty of Engineering, Nagoya Institute of Technology, Nagoya, Japan.

PHASE ANGLE PROPERTIES

To reveal phase angle properties of waveform, suppose that time function f(t) is defined by

$$f(t) = a_o \sin(2\pi f_o t) \qquad 0 \leq t < 16/f_o \qquad (3)$$

It is a harmonic function as shown in Fig. 1.a. The Fourier amplitude takes the value of $8a_o$ at frequency f being equal to f_o by the Fast Fourier Transform computer program used in this study. The corresponding Fourier phase angle lies in the value of -90°. The Fourier amplitudes are zeros at other frequency components, and no specific significance, therefore, is shared with Fourier phase angles.

Let time functions $g_1(t)$, $g_2(t)$ and $g_3(t)$ be defined by

$$g_1(t) = \begin{cases} a_o \sin(2\pi f_o t) & 0 \leq t < 8/f_o \\ 0 & 8/f_o \leq t < 16/f_o \end{cases}$$

$$g_2(t) = \begin{cases} 0 & 0 \leq t < 8/f_o \\ a_o \sin(2\pi f_o t) & 8/f_o \leq t < 16/f_o \end{cases} \qquad (4)$$

$$g_3(t) = \begin{cases} 0 & 0 \leq t < 4/f_o \text{ and } 12/f_o \leq t < 16/f_o \\ a_o \sin(2\pi f_o t) & 4/f_o \leq t < 12/f_o \end{cases}$$

Each waveform is described in Figs. 1.b, 1.c and 1.d, respectively. The Fourier amplitudes of these three waveforms are identical with one another as indicated in Fig. 2.a. Note that the amplitudes in the figure are plotted in a logarithmic scale.

The Fourier phase angle properties of these time functions, however, are quite different with one another. Figures 2.b, 2.c and 2.d illustrate the phase angle properties of functions $g_1(t)$, $g_2(t)$ and $g_3(t)$, respectively. The phase angle at frequency f/f_o being equal to unity is an identical value of -90°, while angles at other frequency components take one of values of 0°, +90°, -90° and -180°, in each waveform.

When analysis has been conducted only upon an aspect concerning Fourier amplitudes so far, these three time functions are concluded to be identical with one another. It is recognized, however, that time functions $g_1(t)$, $g_2(t)$ and $g_3(t)$ in Figs. 2 have different shapes of waveform with one another along their time axis. When considering that earthquake strong motions consist of a number of harmonic motions, Fourier analysis concerned only with their amplitude properties cannot reflect proper significance included in the waveform upon engineering practices. The half amount of informations involved in terms of its Fourier phase angle properties should be taken into account for further analyses of earthquake strong motion records.

Through the inverse Fourier transform, a time function of waveform is reproduced from its Fourier amplitudes and phase angles. It is expected that components corresponding quite different frequencies will individually contribute to the shape of waveform. Neighboring frequency components will interfere and intensity one another. Paying attention upon three major components having largest Fourier amplitudes, a time function is generated. Figures 3.a, 3.b and 3.c represent waveforms corresponding to $g_1(t)$, $g_2(t)$ and $g_3(t)$, respectively. It is concluded that generated functions reproduce

the time varying shape of waveform in good agreement. A similar phenonenom to the "leakage" in the window analysis can be observed. The lower and higher frequency components excluded in reproduction of waveform yield small amplitudes of motion which shall be zeros in the exact inverse Fourier transform.

SIMULATION OF EARTHQUAKE STRONG MOTIONS

Two types of procedures for simulation of earthquake strong motions are introduced. The procedures are both based upon the Fourier transform of a waveform. One, called the Type-I hereafter, is to determine the Fourier phase angle properties from the quantities of a specific motion. The other, the Type-II, is to establish the Fourier amplitude quantities from the analysis upon a specific motion. The former will reflect the significance of Fourier phase angle properties, and the latter will represent the significance of Fourier amplitude properties upon synthetic earthquake strong motions.

Six real earthquake strong motion records are employed for simulation of motions. Three are obtained in the States; accelerograms at El Centro (hereafter abbreviated to ELC) during the Imperial Valley Eq. of 1940, those at Taft (TFT) during the Kern County Eq. of 1952, and those at Pacoima Dam (PCD) during the San Fernando Eq. of 1971. And three in Japan; accelerograms at Hachinohe (HCH) during the Tokachi-Oki Eq. of 1968, those at Tohoku University (THU) during the Miyagi-Ken-Oki Eq. of 1978, and those at Hiroo (HRO) during the Urakawa-Oki Eq. of 1982. Three components, two in horizontal directions and one in vertical direction, in each records are made use of.

Among these accelerograms, the East-West component at Hachinohe is selected for the specific waveform. The time trace of the accelerogram of the HCH EW component is presented in Fig. 4. The accelerogram of the S00E component of ELC and that of the DOWN component of PCD are shown in Figs. 5.

With use of the Type-I procedure reflecting the Fourier phase properties of the HCH EW component and the Fourier amplitude properties of the corresponding earthquake accelerogram, synthetic motions are generated through

$$f(t) \leftrightarrow F(\omega) = A(\omega) \exp[-j\Phi(\omega)] \qquad (5)$$

where

$$\begin{aligned} A(\omega) &= A_{XXX\ YY}(\omega) \\ \Phi(\omega) &= \Phi_{HCH\ EW}(\omega) \end{aligned} \qquad (6)$$

in which "XXX" and "YY" designate the identification of earthquake motion records, i.e. ELC, TFT and so on, and that of the components, i.e. North-South, East-West and Up-Down, respectively.

Similarly, with use of the Type-II procedure representing the Fourier amplitudes properties of the HCH EW component and individual Fourier amplitude properties of the corresponding accelerogram by use of the relation defined by Eq. (5), where, in this simulation,

$$\begin{aligned} A(\omega) &= A_{HCH\ EW}(\omega) \\ \Phi(\omega) &= \Phi_{XXX\ YY}(\omega) \end{aligned} \qquad (7)$$

Simulated earthquake strong motions from Type-I and Type-II procedures are shown in Figs. 6 and 7, respectively, for the ELC S00E and PCD DOWN components.

Two quantities of strong motion records are evaluated. One is the energy of waveform defined by the integration of the square acceleration. The other is the maximum elastic response obtained for a slightly damped SDOF system. These are obtained for both real and synthetic earthquake strong motions. Comparing results from real and synthetic motions with each other, the significance of Fourier phase angle and amplitude properties is described.

Cumulative Energy

Let the energy contained in waveform $f(t)$ during interval $0 \leq t < T$ be defined by the integration of $f(t)$ squared,

$$E(T) = \int_0^T f^2(t)\, dt \qquad (8)$$

Define "the normalized cumulative energy function" [1,2] by

$$e(T) = E(T) / E(T_D) \qquad (9)$$

in which T_D designates an entire duration of motion.

In Fig. 8 , functions for synthetic motions from the Type-I procedure are plotted for the ELC S00E, TFT S69E and PCD DOWN components. These synthetic motions reflect the phase angle properties of the HCH EW component, and its amplitude properties are determined from the corresponding component. The thick curve indicates the function obtained for the real HCH EW motion, and thin curves correspond to those obtained for the synthetic motions. Functions for synthetic motions from the Type-II procedure are shown in Fig. 9. The synthetic motions, in this case, reflect the amplitude properties of the HCH EW component, and its phase angle properties are established from the corresponding component. In this figure, thick curves show results of real components of ECL S00E, TFT S69E and PCD DOWN, respectively, with shift of the time axis by 5 seconds.

Cumulative energy functions for synthetic motions with combination of the HCH EW component and horizontal components of other five earthquake records are determined from a statistical point of view. Figure 10 shows the results for motions from the Type-I procedure, and Fig. 11 from the Type-II procedure. In these figures, the thick solid, the thin solid, and two dashed curves represent the function for the real HCH EW component, the mean value obtained across the synthetic motions, and maximum and minimum values among the synthetic motions, respectively. Shaded zone indicates the variation of three times of standard deviation around the mean value.

Maximum Elastic Response

With a fraction of critical damping of 0.05 associated with the SDOF oscillating system, elastic responses are evaluated. Amplitudes of motion are so linearly scaled that the total energy $E(T_D)$ of motion becomes identical to that of the HCH EW component. Figures 12 indicate the responses for motions from the Type-I procedure for components of ELC S00E and PCD DOWN. Figure 13 describes for motions from the Type-II procedure. Axes x and y represent the undamped natural period and the maximum pseudo velocity response, respectively.

For synthetic motions generated with the HCH EW component and horizontal components of motions, elastic responses are obtained. The mean and the standard deviation across the responses are determined. Figures 14 and 15 describe the statistical results for synthetic motions from the Type-I procedure and from the Type-II procedure, respectively. The legends of curves in the diagrams are identical to those representing the cumulative energy. The shade, however, in the spectral diagrams, identifies the variation of one time of the standard deviation around the mean.

CONCLUDING REMARKS

Synthetic motions generated from a set of real earthquake components reveal characteristic feature. The motions from the Type-I procedure which are reflecting the phase angle properties of a specific motion represent similar forms in the normalized cumulative energy function to that obtained for the specific motion. While disagreement of energy quantities associated with time are found, general tendencies of energy function both for real and synthetic motions coincide well with each other. The poor coincidence of quantities would be caused by the possible "leakage" due to the higher and/or lower frequency components other than dominant components. Provided that phase angle quantities are determined, energy distribution of waveform will be established. The cumulative energy function will be related uniquely to the variation of amplitudes of motion associated with time [1,2]. The Fourier phase angle properties are concluded to be closely related to the intensity of motion along duration of motion.

The motions from the Type-II procedure, containing the identical amplitude properties to that of a specific motion, produce similar responses to those from the specific motion. In an elastic analysis, while distribution of energy along duration of motion differs with one another, responses subjected to the motions are similar. Correspondence between Fourier amplitudes and undamped maximum velocity responses leads to the evidence of the above coincidence.

It is concluded that the phase angle properties will determine the energy distribution of waveform along duration of motion, while the amplitude properties will define the energy distribution associated with frequencies. Mathematically, analysis of earthquake strong motion records with their amplitude properties so far will exclude a half amount of informations which are included in phase angles. It is necessary to reveal features of earthquake strong motions including their phase angle properties for further analyses of earthquake strong motion records.

REFERENCES

[1] Kubo, T. and N. Suzuki, "An Application of Synthetic Earthquake Ground Motions to Response Analysis," Proc. 5th Japan Earthq. Engng Symp., pp. 89-96, November 1978.

[2] Kubo, T. and N. Suzuki, "Generation of Synthetic Earthquake Motions and Their Application to Dynamic Response Analyses," Proc. 7th Wld Conf. on Earthq. Engng, Vol. 2, pp. 333-340, September 1980.

[3] Ohsaki, Y., "On the Significance of Phase Content in Earthquake Ground Motions," Int. J. Earthquake Eng. & Struct. Dynamics, Vol. 7, pp. 427-439, September 1979.

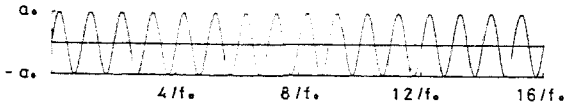

Fig. 1.a Time trace of a harmonic function.

Fig. 1.b Time trace of function $g_1(t)$.

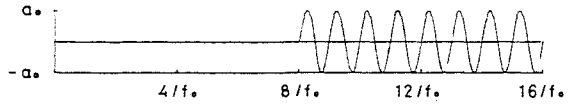

Fig. 1.c Time trace of function $g_2(t)$.

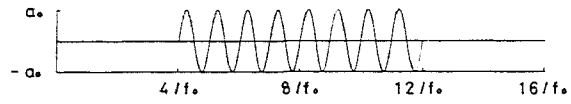

Fig. 1.d Time trace of function $g_3(t)$.

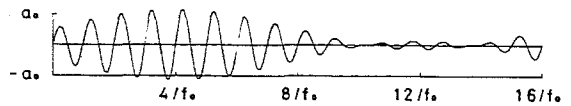

Fig. 3.a Reproduced waveform of $g_1(t)$.

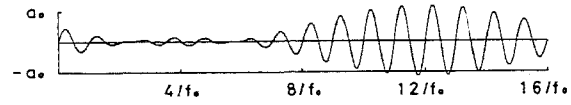

Fig. 3.b Reproduced waveform of $g_2(t)$.

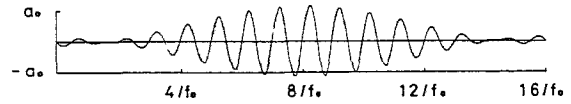

Fig. 3.c Reproduced waveform of $g_3(t)$.

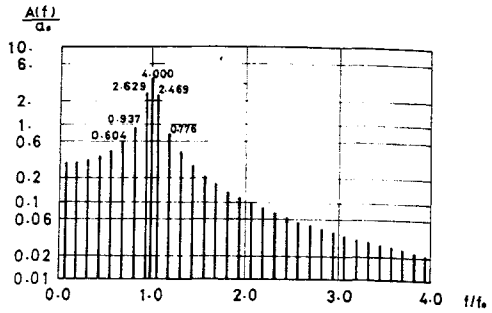

Fig. 2.a Fourier amplitudes.

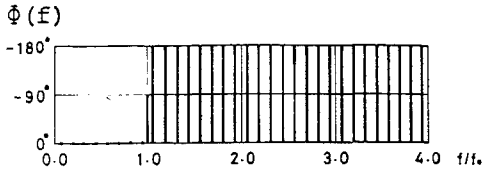

Fig. 2.b Fourier phase angles for function $g_1(t)$.

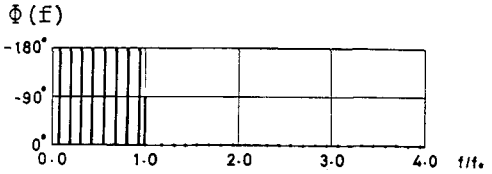

Fig. 2.c Fourier phase angles for function $g_2(t)$.

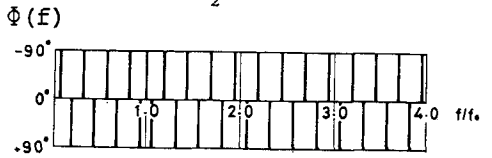

Fig. 2.d Fourier phase angles for function $g_3(t)$.

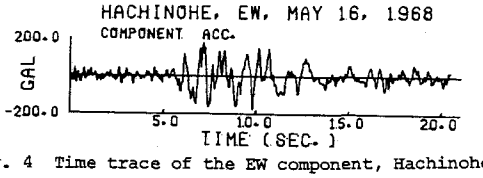

Fig. 4 Time trace of the EW component, Hachinohe.

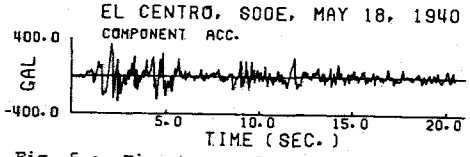

Fig. 5.a Time trace of the S00E component, El Centro.

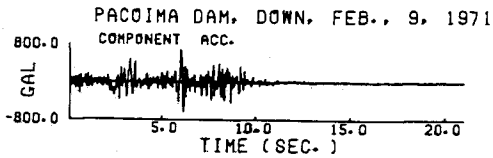

Fig. 5.b Time trace of the DOWN component, Pacoima Dam.

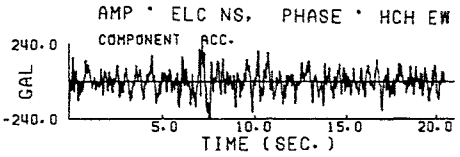

Fig. 6.a Time trace of the synthetic motion, amplitude : ELC S00E and phase : HCH EW.

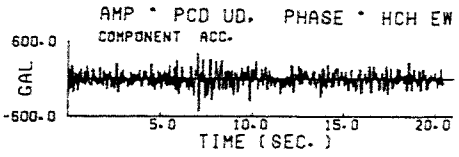

Fig. 6.b Time trace of the synthetic motion, amplitude : PCD DOWN and phase : HCH EW.

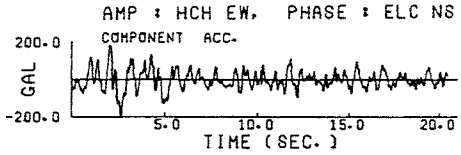

Fig. 7.a Time trace of the synthetic motion, amplitude : HCH EW and phase : ELC S00E.

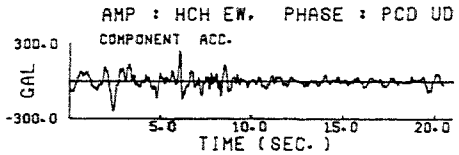

Fig. 7.b Time trace of the synthetic motion, amplitude : HCH EW and phase : PCD DOWN.

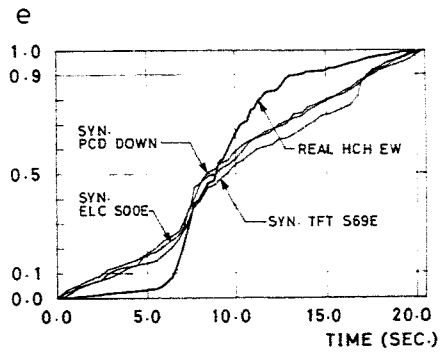

Fig. 8 Normalized cumulative energy for motions from the Type-I procedure, ELC S00E, TFT S69E and PCD DOWN components.

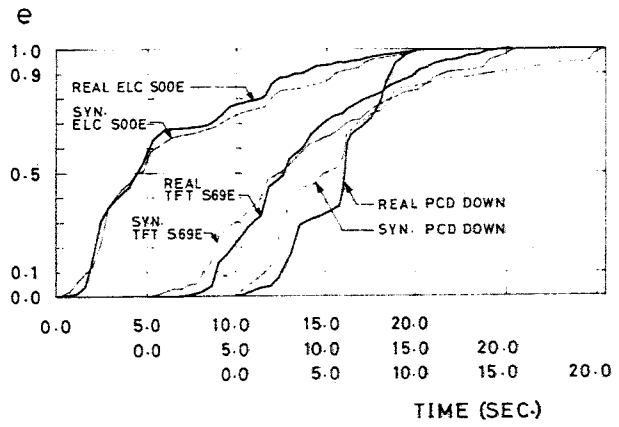

Fig. 9 Normalized cumulative energy for motions from the Type-II procedure, ELC S00E, TFT S69E and PCD DOWN components.

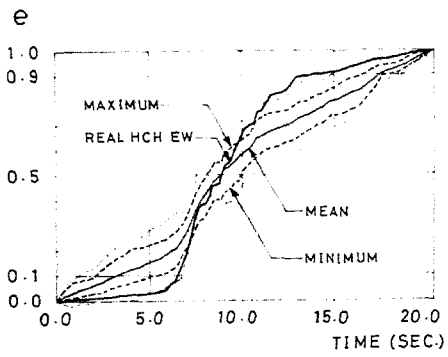

Fig. 10 Normalized cumulative energy for motions from the Type-I procedure.

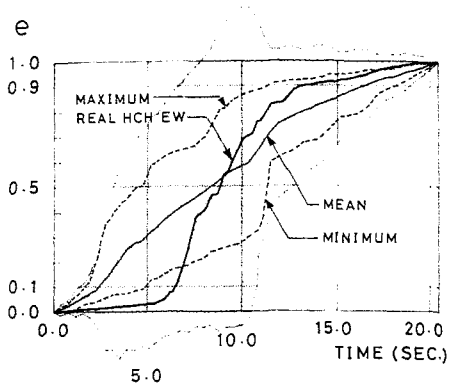

Fig. 11 Normalized cumulative energy for motions from the Type-II procedure.

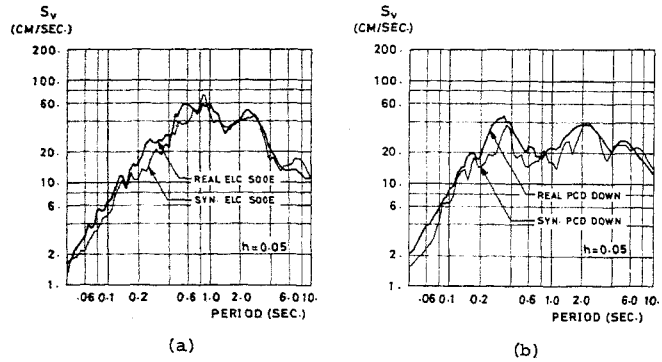

Fig. 12 Elastic responses for motions from the Type-I procedure, ELC S00E and PCD DOWN components.

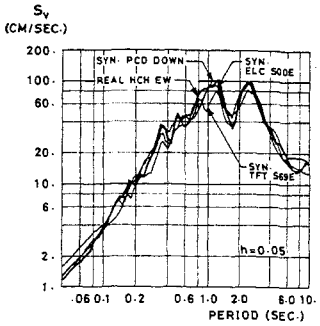

Fig. 13 Elastic responses for motions from the Type-II procedure, ELC S00E, TFT S69E and PCD DOWN components.

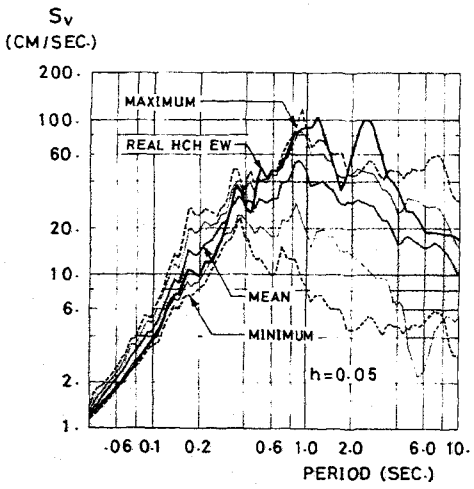

Fig. 14 Elastic responses for motions from the Type-I procedure.

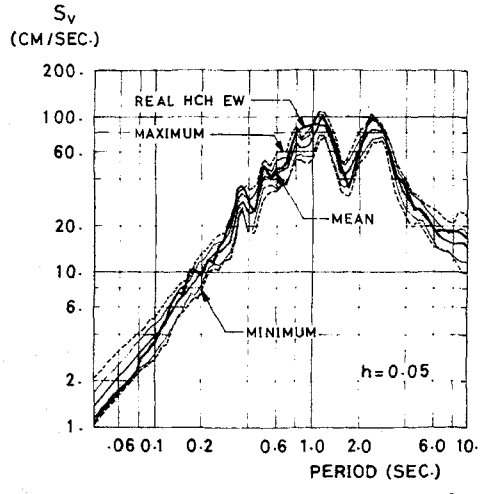

Fig. 15 Elastic responses for motions from the Type-II procedure.